Journal of Molecular Structure 1161 (2018) 285–298

Contents lists available at ScienceDirect

Journal of Molecular Structure

journal homepage: http://www.elsevier.com/locate/molstruc

Synthesis, spectral characterization and X-ray crystal structure studies of 3-(benzo[d][1,3]dioxol-5-yl)-5-(3-methylthiophen-2-yl)-4,5-dihydro-1H-pyrazole-1-carboxamide: Hirshfeld surface, DFT and thermal analysis

Karthik Kumara [a], A. Dileep Kumar [b], S. Naveen [c], K. Ajay Kumar [b], N.K. Lokanath [a, *]

[a] Department of Studies in Physics, Manasagangotri, University of Mysore, Mysuru, 570 006, India
[b] Department of Chemistry, Yuvaraja's College, University of Mysore, Mysuru, 570 005, India
[c] Department of Physics, School of Engineering and Technology, Jain University, Bangalore, 562 112, India

ARTICLE INFO

Article history:
Received 11 November 2017
Received in revised form
15 February 2018
Accepted 15 February 2018
Available online 19 February 2018

Keywords:
Claisen-schmidt reaction
Pyrazole carboxamide
X-ray diffraction
Self-assembly
Hirshfeld surface
DFT/B3LYP

ABSTRACT

A novel pyrazole derivative, 3-(benzo[d][1,3]dioxol-5-yl)-5-(3-methylthiophen-2-yl)-4,5-dihydro-1H-pyrazole-1-carboxamide was synthesized and characterized by elemental analysis, FT-IR, NMR (^{1}H and ^{13}C), MS, UV–visible spectra and finally the structure was confirmed by the single crystal X-ray diffraction studies. The title compound ($C_{16}H_{15}N_3O_3S$) crystallized in the triclinic crystal system, with the space group *Pi*. A dihedral angle of 65.84(1)° between the pyrazole and the thiophene rings confirms the twisted conformation between them. The X-ray structure revealed that the pyrazole ring adopts an *E*-form and an envelope conformation on C7 atom. The crystal and molecular structure of the title compound is stabilized by inter molecular hydrogen bonds. The compound possesses three dimensional supramolecular self-assembly, in which C—H···O and N—H···O chains build up two dimensional arrays, which are extended to 3D network through C—H···*Cg* and C—O···*Cg* interactions. The structure also exhibits intramolecular hydrogen bonds of the type N—H···N and π···π stacking interactions, which contributes to the crystal packing. Further, Hirshfeld surface analysis was carried out for the graphical visualization of several short intermolecular interactions on the molecular surface while the 2D fingerprint plot provides percentage contribution of each individual atom-to-atom interactions. The thermal decomposition of the compound has been studied by thermogravimetric analysis. The molecular geometries and electronic structures of the compounds were fully optimized, calculated with ab-initio methods by HF, DFT/B3LYP functional in combination of different basis set with different solvent environment and the structural parameters were compared with the experimental data. The Mulliken atomic charges and molecular electrostatic potential on molecular van der Waals (vdW) surface were calculated to know the electrophilic and nucleophilic regions of the molecular surface. Nonlinear optical properties of the title compound were also discussed based on the polarizability and hyperpolarizability values.

© 2018 Elsevier B.V. All rights reserved.

1. Introduction

Design and development of an accessible procedure for the synthesis of simple heterocycles with various functionalities is a worthwhile contribution in organic synthesis. The compounds with pyrazole moieties are the most prominent class in active pharmaceutical drugs and agrochemicals in controlling infections, diseases and pests [1]. Pyrazoline carboxamide are the classical compounds having active functional pyrazoline and amide group. These two groups plays vital role in the drug action. Pyrazoline carboxamide and thiocarboxamide inhibit monoamine oxidases (family of enzymes present in prokaryotic and eukaryotic organisms that oxidatively catalyzes monoamines). The dipole moment of these compounds revealed that the C=S group is more polarizable than the C=O group [2]. Both thio and carbonyl group in N11 position of pyrazoline moiety appears to be very effective towards the biological activity. Pyrazole derivatives with electron donating and withdrawing substituents modulate the biological activity [3].

* Corresponding author.
E-mail address: lokanath@physics.uni-mysore.ac.in (N.K. Lokanath).

https://doi.org/10.1016/j.molstruc.2018.02.068
0022-2860/© 2018 Elsevier B.V. All rights reserved.

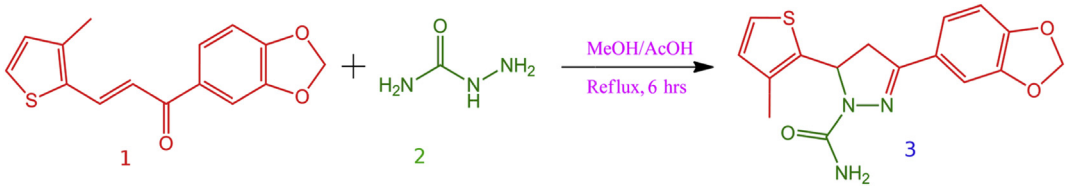

Scheme 1. Reaction pathway for the synthesis of the title compound.

Chalcones having α, β-unsaturated ketone group embedded between two aromatic rings are of immense importance in the construction of biologically active molecules. These chalcones are the precursor for the synthesis of various heterocyclic compounds like benzothiazepines [4], pyrazoles [5], isoxazoles [6] pyrazole carboxamide [7] cyclopropyl esters, [8]. In view of these synthetic utilities and biological activities associated with α, β-unsaturated ketones and the pyrazole derivatives, we have synthesized the title compound by the reaction of (*E*)-1-(benzo[*d*] [1,3]dioxol-5-yl)-3-(3-methyltiophene-2-yl)prop-2-en-1-one (**1**) with semicarbazide hydrochloride to yield the pyrazole carboxamide. The compound (1) was synthesized by Claisen-Schmidt condensation reaction between 3-methylthiophene-2-carbaldehyde and 1-(benzo[d] [1,3] dioxol-5-yl) ethanone in the presence of potassium hydroxide with ethanol solvent. As a part of our on-going research work on pyrazole derivatives, we herein report the synthesis, spectral characterization and single crystal X-ray diffraction studies of novel 3-(benzo[d] [1,3]dioxol-5-yl)-5-(3-methylthiophen-2-yl)-4,5-dihydro-1H-pyrazole-1-carboxamide formed by 3 + 2 cycloaddition of thiophene appended chalcone with semicarbazide. Further, Hirshfeld surface analysis was carried out extensively to understand the intermolecular interactions. The thermal stability of the title compound was studied through thermogravimetric analysis. Density functional theory (DFT) was used to perform the geometry optimization and calculations of the electronic spectra for exploring the non-linear optical (NLO) applications of the title compound.

2. Experimental

2.1. Materials and methods

All the chemicals were purchased from commercial suppliers (Sigma Aldrich) and were used without further purification. Melting points were determined by an open capillary tube method. Purity of the compound was checked on thin layer chromatography (TLC) plates pre-coated with silica gel using solvent system hexane**:** ethyl acetate (1:4). The spots were visualized under UV light. ^{1}H and ^{13}C NMR spectra were recorded on Agilent-NMR 400 MHz and 100 MHz spectrometer respectively. The solvent $CDCl_3$, with TMS as an internal standard, was used to record the spectra. The chemical shifts are expressed in δ ppm. Mass spectrum was obtained on Mass Lynx SCN781 spectrometer TOF mode. Elemental analysis was obtained on a Thermo Finnigan Flash EA 1112 CHN analyzer. The IR spectrum was recorded by the potassium bromide pellet method on FT-IR Agilent spectrophotometer. The UV–visible absorption spectrum was recorded using Shimadzu UV-1800 spectrophotometer. The thermogravimetric analysis (TGA) was carried out by using Perkin Elmer Pyris TGA instrument.

2.2. Synthesis

To the solution of (*E*)-1-(benzo[*d*][1,3]dioxol-5-yl)-3-(3-methyltiophene-2-yl)prop-2-en-1-one (**1**) (2.721 g, 10 mmol) and semicarbazide hydrochloride (**2**) (3.34 g, 30 mmol) dissolved in methanol (5–7 ml), glacial acetic acid (6–8 ml) was added; the mixture was refluxed for 6 h in an oil bath. The progress of the reaction was monitored by TLC. After completion of the reaction, the mixture was poured into ice cold water. The solid separated was filtered, washed with ice cold water to remove excess semicarbazide, dried in vacuum chamber to obtain the crude product. Colorless rectangular slab like crystals (yield was 84%) of the title compound were grown by slow evaporation method using ethyl acetate (1 ml), methanol (1 ml) and acetonitrile (2 drops) mixture solvents. The synthetic pathway of the reaction is depicted in Scheme 1.

2.3. Computational details

The molecular geometry optimization and the vibrational frequency calculations of the title compound were carried out using *Gaussian* 09 software suit [9]. Initially the X-ray structure coordinates were used as starting point for the ground state geometry optimization using Hartree-Fock (HF) and DFT with the Becke-3-parameter-Lee-Yang-Parr (B3LYP) functional [10,11] levels for the 3-21 + G, 6-31 + G(d,p) and 6-311 + G(d,p) basis sets. The DFT/B3LYP level of theory with 6-31 + G(d,p) basis set is extensively used to carry out the theoretical calculations of the molecule with different solvent environment to study and compare the solvent effect on structural parameters of the molecule. The Mulliken atomic charges, HOMO, LUMO energies and their energy gap were calculated. The electronic absorption spectrum was investigated using the TD-DFT [12,13] with B3LYP functional for solvent and gas phase. Further, dipole moment (μ), nonlinear optical (NLO) properties, linear polarizabilities (α) and first hyperpolarizabilities (β) have also been studied. *Chemcraft* [14] software is used to visualize the optimized structures. The molecular electrostatic potential (MEP) map and frontier molecular orbitals (FMO) were drawn using Gauss-View 5.0.8 [15] software. *Crystal Explorer* 3.1 [16] program was used for the Hirshfeld surface analysis and its calculations.

2.4. Crystallographic analysis

Rectangular shaped colourless defect free single crystal of approximate dimension 0.43 × 0.36 × 0.29 mm^3 was chosen for X-ray diffraction studies. X-ray intensity data for the title compound was collected at temperature 293 K on Rigaku XtaLAB Mini diffractometer with X-ray generator operating at 50 kV and 12 mA, using MoK_α radiation of wavelength 0.71073 Å. Data were collected with χ fixed at 54° and for different settings of φ (0° and 360°), keeping the scan width of 0.5°, exposure time of 3 s, the sample to detector distance of 50 mm. The compound $C_{16}H_{15}N_3O_3S$ crystallized in the triclinic crystal system, in *P*$\bar{1}$ space group. The complete intensity data sets were processed using *CRYSTAL CLEAR* [17]. The crystal structure was solved by direct method and refined by full-matrix least squares method on F^2 using *SHELXS* and *SHELXL* programs [18], respectively. All the non-hydrogen atoms were refined anisotropically and the hydrogen atoms were positioned

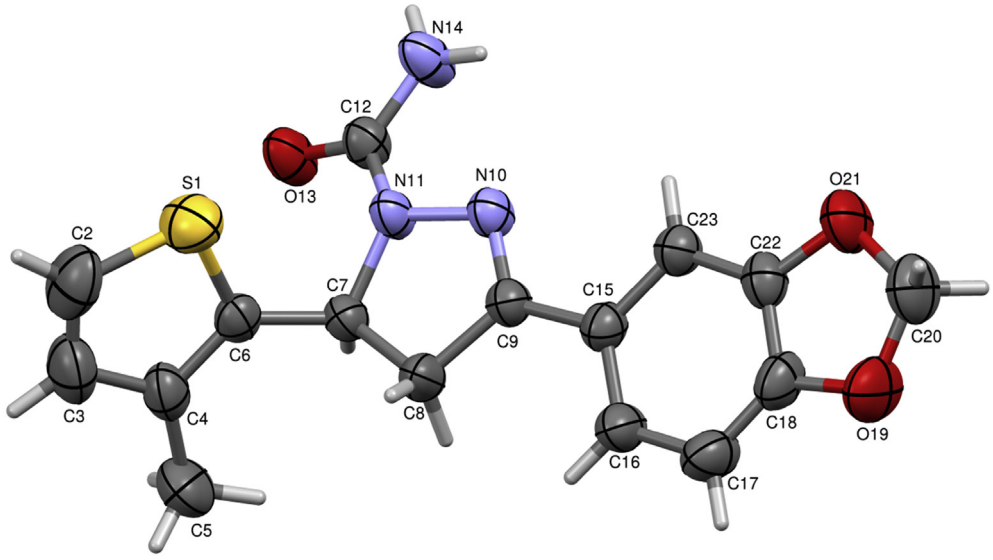

Fig. 1. ORTEP diagram of the molecule with thermal ellipsoids drawn at 50% probability.

geometrically, with C–H = 0.93–0.97 Å and refined using a riding model with U_{iso}(H) = 1.2 U_{eq}(C, N), U_{iso}(H) = 1.5 U_{eq} (C_{methyl}). A total of 209 parameters were refined with 2647 unique reflections of 3697 observed reflections. After several cycles of refinement, the final difference Fourier map showed peaks of no chemical significance and the residual value was saturated to 0.0507. The geometrical calculations were performed using *PLATON* [19]. The molecular and packing diagrams were generated using the software *MERCURY* [20]. The ORTEP of the molecule with displacement ellipsoids drawn at 50% probability level is shown in Fig. 1. The details of the crystal data and structure refinement are as given in Table 1.

Table 1
Crystal data and structure refinement statistics.

Parameter	value
CCDC deposit No.	1557003
Empirical formula	$C_{16}H_{15}N_3O_3S$
Formula weight	329.37
Temperature	293 K
Wavelength	0.71073 Å
Crystal system, space group	Triclinic, $P\bar{1}$
Unit cell dimensions	$a = 6.364(8)$ Å
	$b = 11.507(13)$ Å
	$c = 11.838(13)$ Å
	$\alpha = 69.58(3)^o$
	$\beta = 82.09(3)^o$
	$\gamma = 86.54(4)^o$
Volume	804.6(16) $Å^3$
Z	2
Density(calculated)	1.359 Mg m^{-3}
Absorption coefficient	0.219 mm^{-1}
F_{000}	344
Crystal size	0.43 × 0.36 × 0.29 mm^3
θ range for data collection	3.07° to 24.4°
Index ranges	$-7 \le h \le 7$
	$-13 \le k \le 10$
	$-13 \le l \le 13$
Reflections collected	3697
Independent reflections	2647 [$R_{int} = 0.0373$]
Absorption correction	multi-scan
Refinement method	Full matrix least-squares on F^2
Data/restraints/parameters	2647/0/209
Goodness-of-fit on F^2	1.034
Final [$I > 2\sigma(I)$]	$R1 = 0.0507$, $wR2 = 0.1335$
R indices (all data)	$R1 = 0.0617$, $wR2 = 0.1455$
Largest diff. peak and hole	0.360 and −0.325 e $Å^{-3}$

3. Results and discussion

3.1. Spectral studies

In order to confirm the formation of the synthesized compound of destination, various spectrochemical methods such as FT-IR, Mass spectra, NMR (^{1}H and ^{13}C) and UV–visible spectra were performed.

3.1.1. NMR spectra

^{1}H NMR spectrum of the title compound showed a singlet peak at δ 2.191 ppm for methyl group. The two methylene protons of the pyrazole ring C_4-H_a and C_4-H_b exhibits diastereotopic nature and appear as a doublet of doublets. C_4-H_a appears as doublet of doublet in the region δ 2.999–3.056 ppm (dd, 1H, C_4-H_a, J = 5.2, 17.6 Hz), while that of C_4-H_b in the region δ 3.701–3.775 (dd, 1H, C_4-H_b, J = 12.0, 18 Hz), C_5-H_c couples not only with C_4-H_a but also with C_4-H_b and appears as doublet of doublet in the region δ 5.599–5.642 (dd, 1H, C_5-H_c, J = 5.2, 11.6 Hz) instead of an expected triplet. The NH_2 protons of the amide group and methylene protons of the piperinal group show two singlets at 6.048 ppm and 6.429 ppm respectively. The thiophene ring with ortho substitution, the two protons in the ring appeared as two doublets in the aromatic region 6.757 and 6.926. Further an array of signals in the region 7.145–7.183 ppm as multiplet and 7.476 ppm as singlet were assigned to three aromatic protons.

In the ^{13}C NMR spectrum, carbon signal at 18.632 is due to methyl group. C-7, C-8 and C-9 carbons of the newly formed pyrazole ring shows the signal at δ 47.309, 59.353 and 152.868 ppm. The other carbon signal for methylene proton is at 106.562. The signals appears for one carbon each at δ 111.024, 113.285, 126.573, 127.4, 130.868, 135.095, 137.509, 145.598, 153.817, 155.486 ppm. The carbonyl carbon for the amide group gives signal at δ 160.131 ppm. The ^{1}H NMR and ^{13}C NMR spctra are given in Fig. S1 and Fig. S2 of the supplementary section.

3.1.2. LCMS study

The mass spectrum showed an M+ peak at m/e 330.03 with a relative abundance of 100% corresponding to base peak at m/z

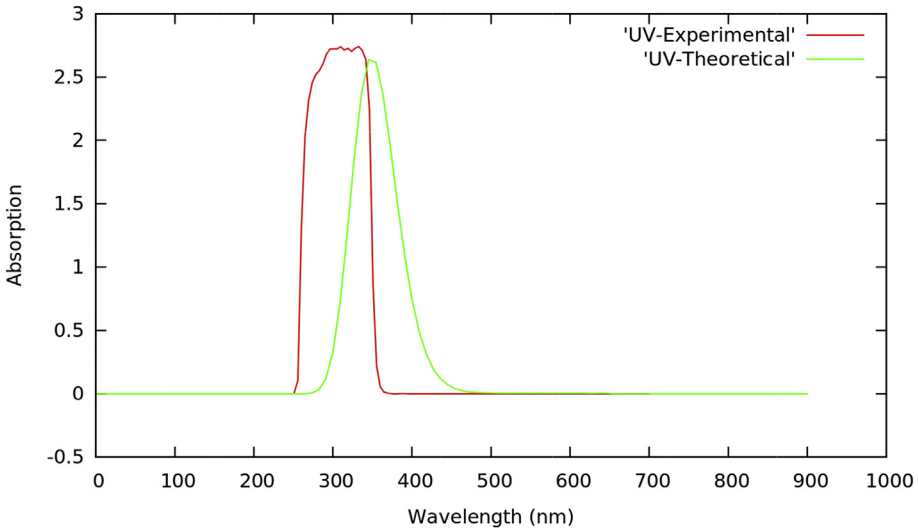

Fig. 2. UV–visible absorption spectrum of the title compound.

329.4 which corresponds to the molecular mass of the title compound. The mass spectral data shows good agreement with expected molecular weight. The mass spectrum is shown in Fig. S3.

3.1.3. FT-IR analysis

In FT-IR spectrum the strong absorption band in the region 3400 cm^{-1} indicates the presence of amide NH_2 group. The IR spectrum of the title compound showed a broad band at 3400 cm^{-1} attributed to amide NH_2 group, two strong bands at 1679 cm^{-1} and 1607 cm^{-1} referring to carbonyl and carbon-carbon double bonds. The experimentally obtained spectrum is compared with the theoretically calculated values and is given in Figs. S4 and. S5 respectively. The significant normal vibrational frequencies and their assignments are given in Table S1 of supplementary section.

3.1.4. Optical absorption by UV–visible spectrum

Electronic absorption spectra of organic compounds are based on the excitation of π electrons to the π^* (excited) state, which occurs in the UV–Vis region. The UV–visible spectrum was recorded for the grown crystal in the range of 250–700 nm. The optical absorption spectrum of the title compound is shown in Fig. 2 and was recorded using DMSO solvent. The spectrum evidences the strong absorption in the region 265–360 nm. The optical band gap energy ($1240/\lambda = 4.2034$ eV) of the grown crystal was calculated using the lower cut-off wavelength (295 nm). This optimum band gap energy may have potential optoelectronic applications due to strong absorption in the near ultraviolet region [21]. The theoretically calculated band gap energy (4.2116 eV) is in very good correlation with the experimentally determined value.

3.2. X-ray crystal structure

The molecular structure of the title compound has been confirmed by single crystal X-ray diffraction analysis. The bond lengths and bond angles are in good agreement with the standard values and are given in Tables S2 and S3 respectively. The observed bond distance of N10–C9 is 1.290(3) Å and O13–C12 is 1.228(3) Å which are consistent with the C=N [22] and C=O character with the standard bond distance [23]. The bond distance 1.390(3) Å of N10–N11 is comparable with the standard bond distance value of 1.35 Å. The list of torsion angles is given in Table S4.

In the molecular structure, the five membered thiophene ring and the five membered pyrazole ring are connected by C–C single bond with a bond distance of 1.498(4) Å. Nine membered benzodioxole ring is connected to the 3-position of the pyrazole ring. The torsion angles of −17.2(3)° (N10–N11–C12–N14) and 164.6(2)° (N10–N11–C12–O13) indicates that the segments C12–N14 and C12–O13 are respectively in the *-syn-periplanar* and an + *anti-periplanar* conformation. Thus the functional amidogen and oxygen atoms are twisted out of the mean plane of the pyrazole ring (N10/N11/C7/C8/C9).

A dihedral angle of 65.84(1)° formed by the mean plane of thiophene ring S1/C2/C3/C4/C6 with the pyrazole ring indicates that the thiophene ring is twisted from the mean plane of the pyrazole ring. Similarly, the benzodioxole ring is almost planar with the mean plane of the pyrazole ring, which is indicated by the dihedral angle of 2.26(1)°. The pyarazole ring adopts an *E*-form with the Cremer and Pople [24] puckering parameters Q = 0.095(3) Å and $\phi = 70.7(1)^o$. The ring puckering analysis reveals that the ring has a weighted average ring bond distance of 1.4254 Å and weighted average torsion angle of 6.26°. The ring also take up an envelope conformation on C7 atom with the pseudo rotation parameters [25] value, P = 230.2(1)° and $\tau = 10.0(2)°$.

The molecule exhibit C–H··· π interaction; C2–H2···*Cg*4 ((Fig. 3) *Cg*4 is the centroid of the ring C15/C16/C17/C18/C22/C23) with a C—*Cg* distance of 3.607(6) Å, H···*Cg* distance of 2.73 Å, C–H···*Cg* angle of 157°, and with a symmetry code *-x*, 1-*y*, 1-*z*. The molecules also exhibit *Cg*···*Cg* interaction; *Cg*3···*Cg*1 ((Fig. 4) *Cg*3 is the centroid of the ring N10/N11/C7/C8/C9 and *Cg*1 is the centroid of the ring S1/C2/C3/C4/C6) with a *Cg*—*Cg* distance of 3.744(5) Å, $\alpha = 65.84(2)°$, $\beta = 59.6°$, $\gamma = 81.6°$, a perpendicular distance of *Cg*3 on ring S1/C2/C3/C4/C6 = 0.5465(1) Å, a perpendicular distance of *Cg*1 on ring N10/N11/C7/C8/C9 = 1.8953(1) Å, and symmetry code *x, y, z*. In the crystal structure, N–H···O hydrogen bonds connect the molecules into inversion dimers. These molecules are further connected through inter and intra molecular C–H···O and N–H···N hydrogen bond interactions [26] forming a three-dimensional network. The hydrogen bonding geometry is listed in Table 2. The packing of molecules when viewed down along *a*-axis shown in Fig. 5 revealed that the molecules form layered stacking along (0 1 0) plane. The bridging of molecules through N–H···O hydrogen bond interactions between amidogen and oxygen element results in an $R_2^2(8)$ ring motif [27] to form supramolecular self-assemblies (Fig. 6).

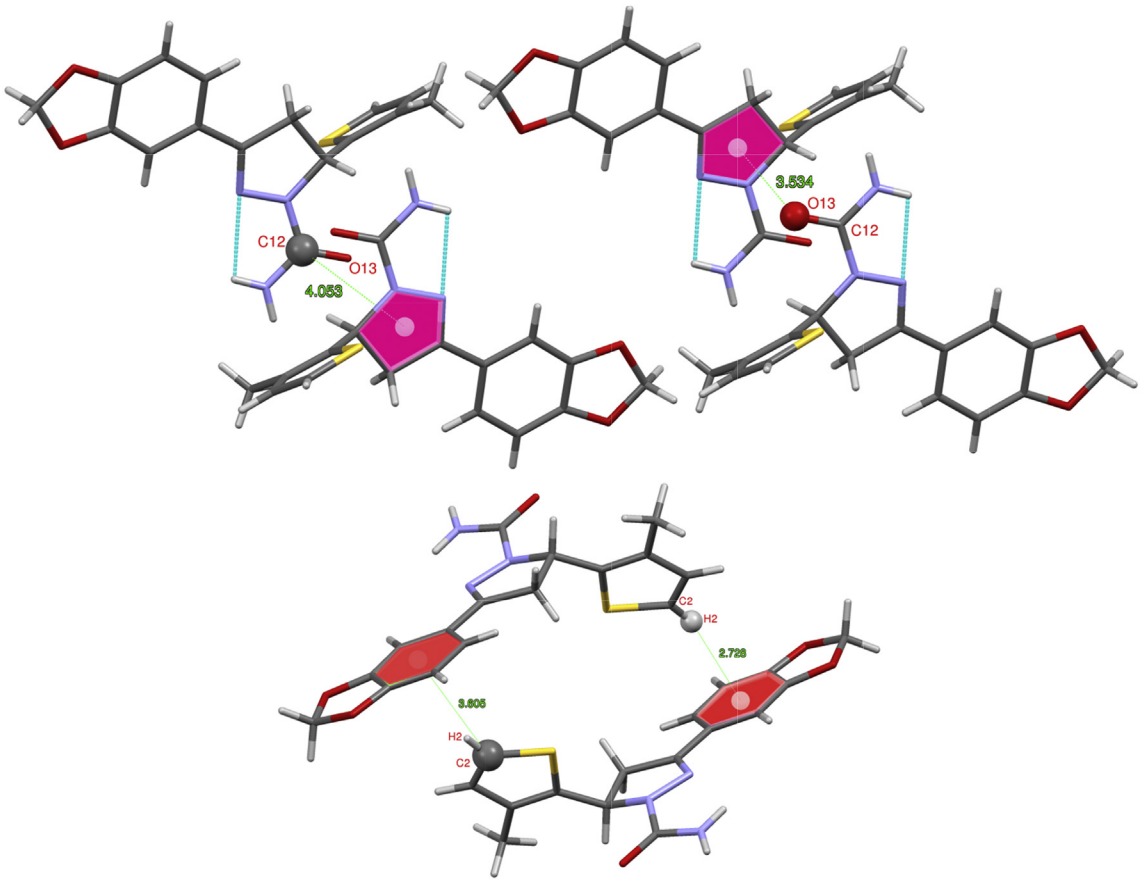

Fig. 3. The molecules exhibit C—H··· π and C—O··· π interactions.

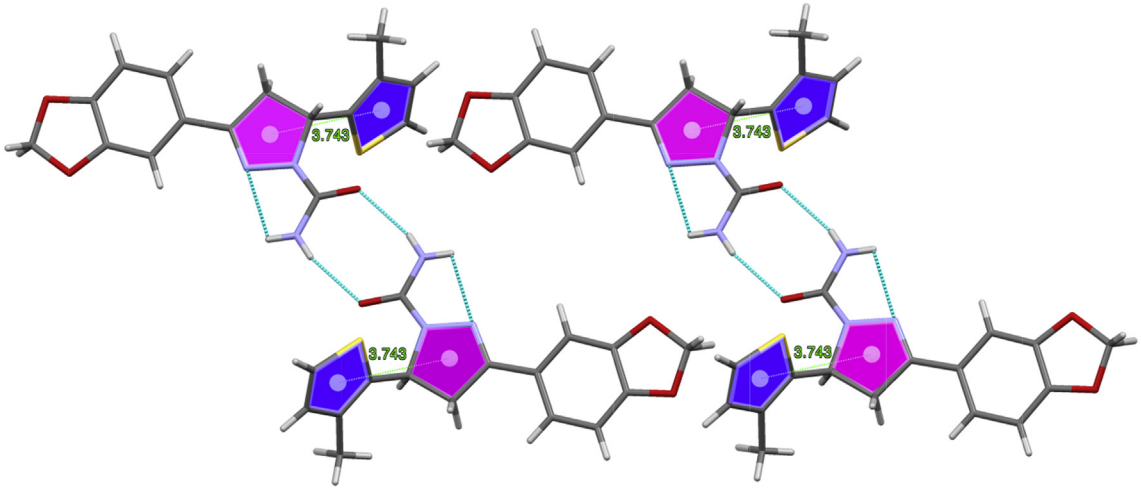

Fig. 4. The molecules exhibiting π··· π interactions.

3.3. Hirshfeld surface studies

Hirshfeld surface analysis (HSA) is a powerful tool for the calculation and the graphical visualization of the intermolecular interactions in the solved crystal structure. HSA is very unique for each crystal structures and was carried out by uploading crystallographic information file (CIF) to the *Crystal Explorer* version 3.1 software. The d_{norm} plot was mapped on Hirshfeld surface with

Table 2
Geometric parameters for hydrogen bond interactions (Å,°).

D—H … A	D—H	H … A	D … A	D—H … A
N(14)—H(14B)···N(10)[c]	0.86	2.10	2.708(4)	104
N(14)—H(14A) … O(13)[i]	0.86	2.36	2.916(5)	157
C(5)—H(5A) … O(19)[ii]	0.96	2.59	3.390(6)	141

[i] 1-x, -y, 1-z.
[ii] 1 + x, y, −1+z.
[c] Intra.

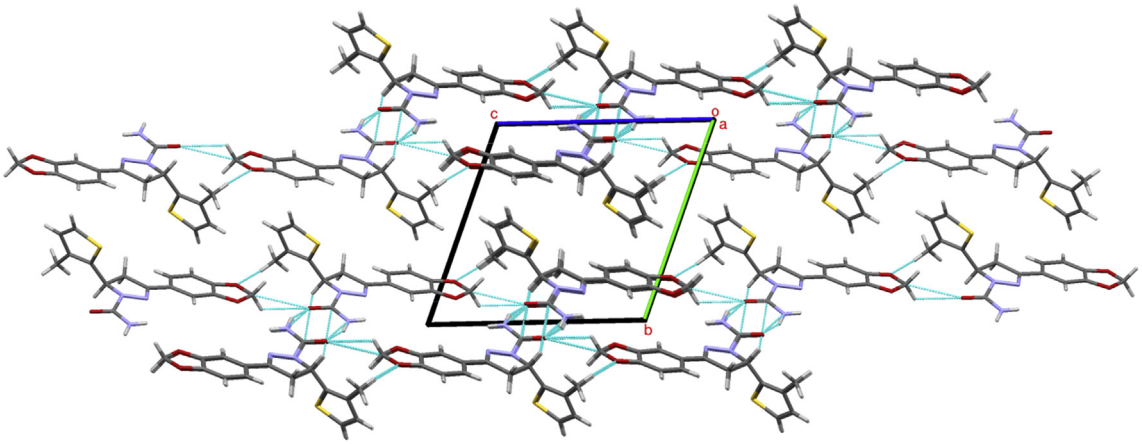

Fig. 5. Packing of the molecules when viewed down along the *a*-axis. The dotted line represents hydrogen bond interactions.

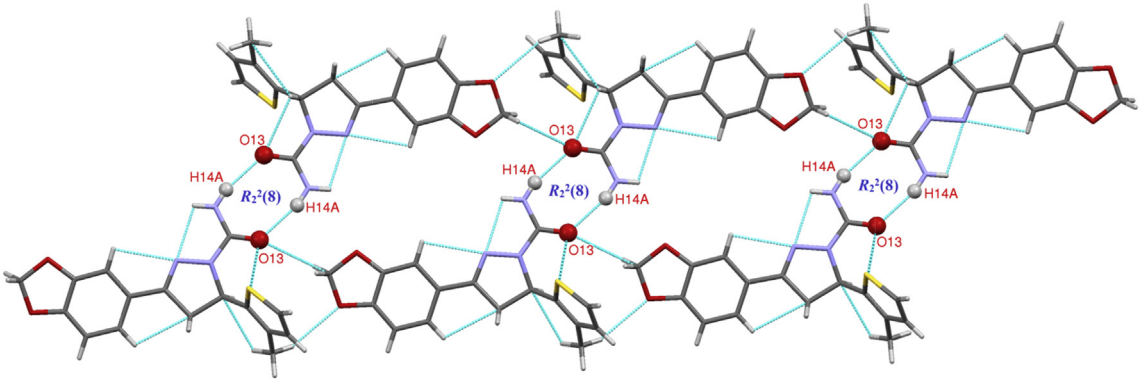

Fig. 6. The supramolecular self-assembly through $R_2^2(8)$ ring motif by N–H···O hydrogen bond interactions between amidogen and oxygen element.

colour scale in between −0.495 au (blue) to 1.616 au (red) respectively. The colour codes on the surface can be used for the analysis of the molecular contacts, such that regions with red and blue colour on the d_{norm} represent the shorter and longer inter contacts, the white colour indicates the contacts around the van der Waals radii [28–30].

The calculated volume inside the Hirshfeld surface is 395.05 $Å^3$ in the area of 353.28 $Å^2$ with globularity (G) 0.737 as well as asphericity (Ω) 0.238. The overall calculation is performed with the TONTO [31] integrated with Crystal Explorer.

Fig. 7 represents two dimensional fingerprint plots (FP) [32,33] with de and di distances in the range 0.6–2.8 Å display different intermolecular interactions. Where d_i is the closest internal distance from a given point on the Hirshfeld surface and d_e is the closest external contacts. The FP reveals the contribution of each individual intermolecular contact to the surface which can be identified through colour codes (frequency of presence). If $d_i > d_e$ then this represents the dark regions on the surface are due to interaction of hydrogen bond acceptors. Similarly, the regions with $d_e > d_i$ value are due to the hydrogen bond acceptors. The white colour indicates no occurrence, blue indicates some occurrence and green then red indicates more frequent occurrence of any given (d_i, d_e) pair. From the total contributions the H···H contacts has maximum and C···N has minimum contributions. Similarly the C···H, O···H, N···H and S···H contacts also contribute to the total area of the surface as shown in Fig. 8.

The C–H···π and π···π interactions are evidently given in fingerprint plots. The two of spikes with points at d_e and d_i in the FP illustrate that the value of ($d_e + d_i = 1.1 + 1.7$) is 2.8 Å for C ···H interactions and ($d_e + d_i = 0.8 + 1.16$) 1.96 Å for O ···H (Fig. 9) interactions in the donor and acceptor regions of the FP. The inter-contact distances obtained from Hirshfeld analysis are in good correlation with the single crystal analysis.

These contacts are highlighted on the molecular surface using conventional mapping of d_{norm}, shape index and curvedness as shown in Fig. 10. The dark red regions on the d_{norm} surface are due to short inter contacts (strong hydrogen bonds), while the other interactions are appear as light-red spots. The red concave region on shape index is the surface around the acceptor atom and the blue region is the surface around the donor atoms. The adjacent red-blue triangles indicates the identical π···π stacking interactions over the surface. Curvedness is the root mean square value of the curvature of the surface. The value of curvedness (low with flat area and high with sharp curvature) divide the surface into contact patches with the nearest molecule. The flat regions of the surface indicates the π ··· π stacking interactions [34,35].

3.4. DFT optimized structures and molecular orbitals

The calculated optimized structure of the title compound is shown in Fig. 11. The bond lengths and bond angles calculated using ab-initio methods HF/3-21G [36] and HF/6-31G* [37] along with

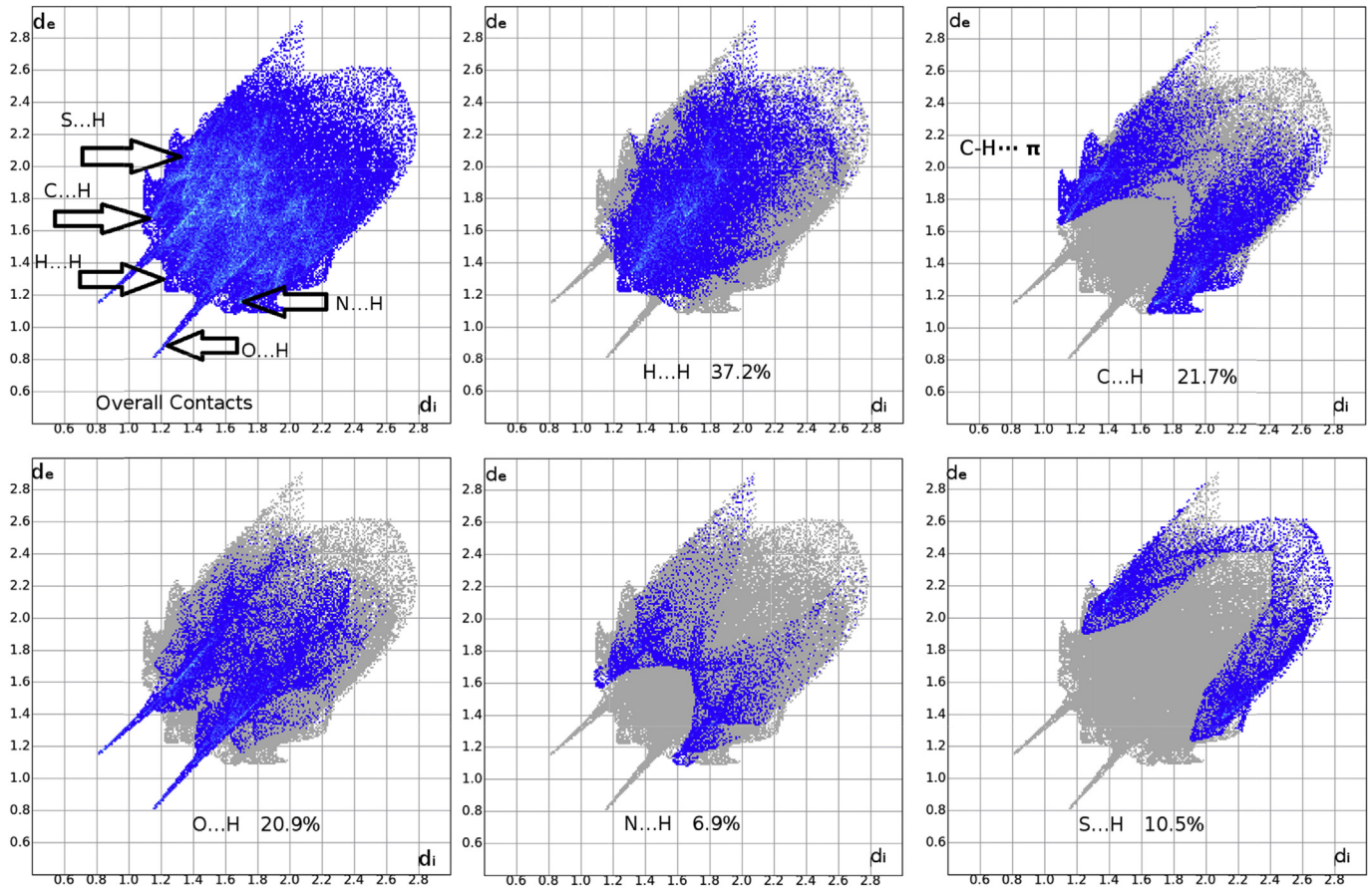

Fig. 7. Fingerprint plots and corresponding surface area of the title compound showing the individual contribution of each interaction.

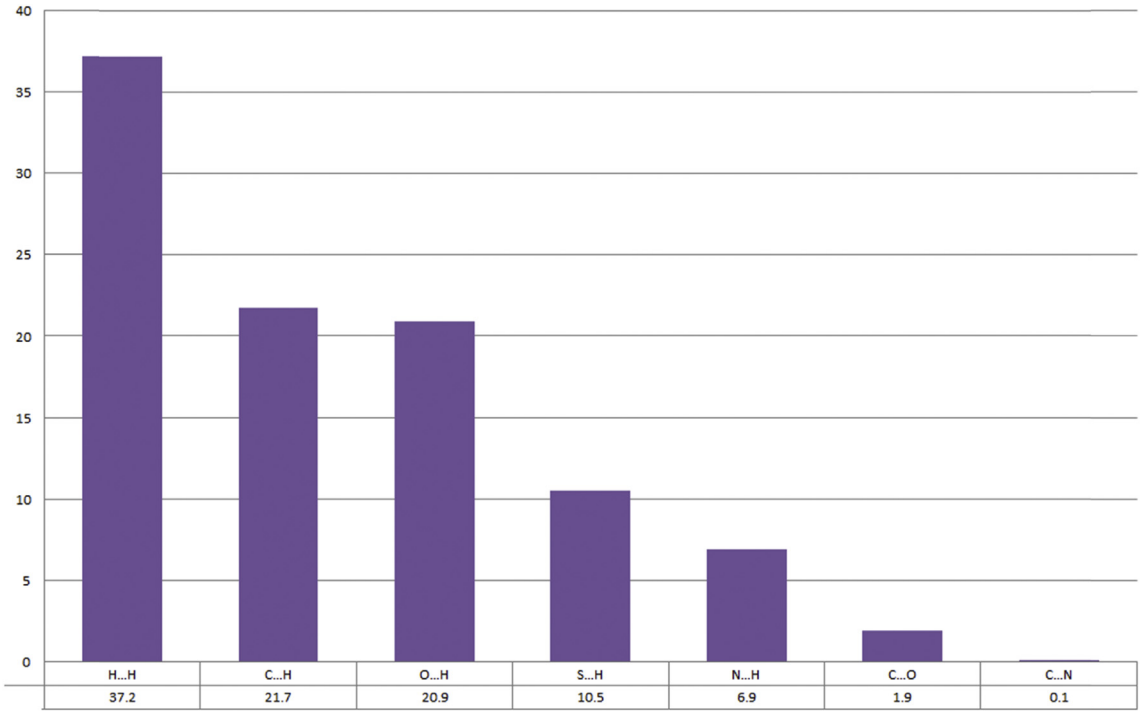

Fig. 8. Individual contributions of intermolecular interactions to the total area of the surfaces in the title compound.

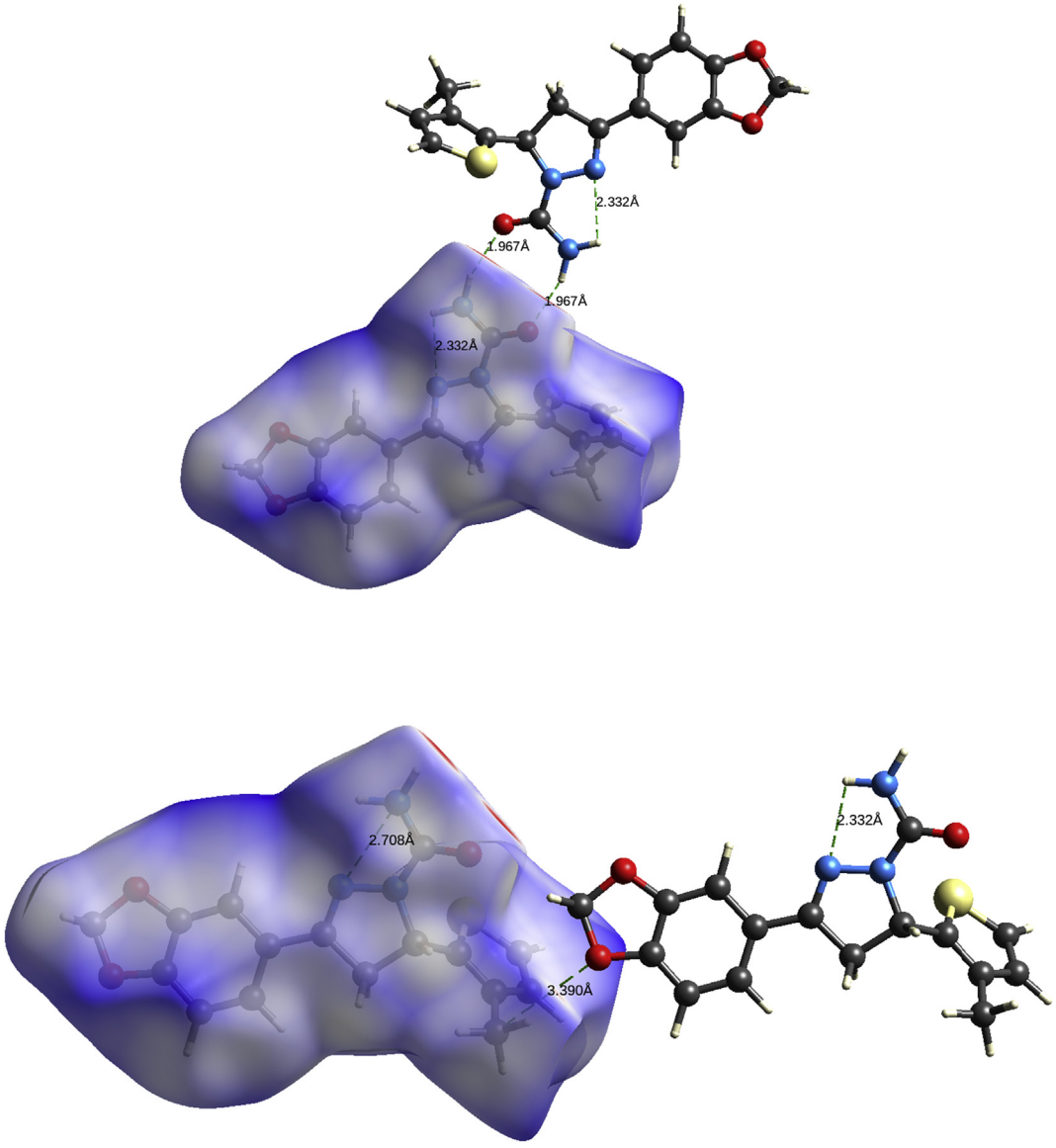

Fig. 9. Molecular interactions on Hirshfeld surface.

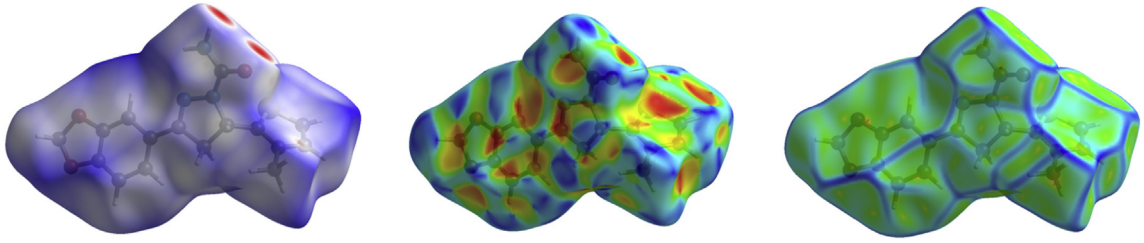

Fig. 10. dnorm, shape index and curvedness mapped on Hirshfeld surface visualizing the molecular contacts.

the most commonly used B3LYP/6-31G*, B3LYP/6-311G* [38–42] basis set with different solvent environment were given in Table 3. The correlation coefficient (CC) for bond lengths obtained at HF/3-21G, HF/6-31G* and B3LYP/6-31G* are 0.9895, 0.9922 and 0.9923 respectively. Similarly, the CC for bond angles are 0.9859, 0.9929 and 0.9934 for HF/3-21G, HF/6-31G* and B3LYP/6-31G*. Though all the methods gave high correlation coefficient values for the bond lengths and bond angles, B3LYP/6-31G* method with acetone solvent environment gives the highest correlation coefficients when compared with the other solvent effect. The graphical correlation between the experimentally determined bond lengths and bond angles versus theoretically calculated values by HF/3-21G, HF/6-

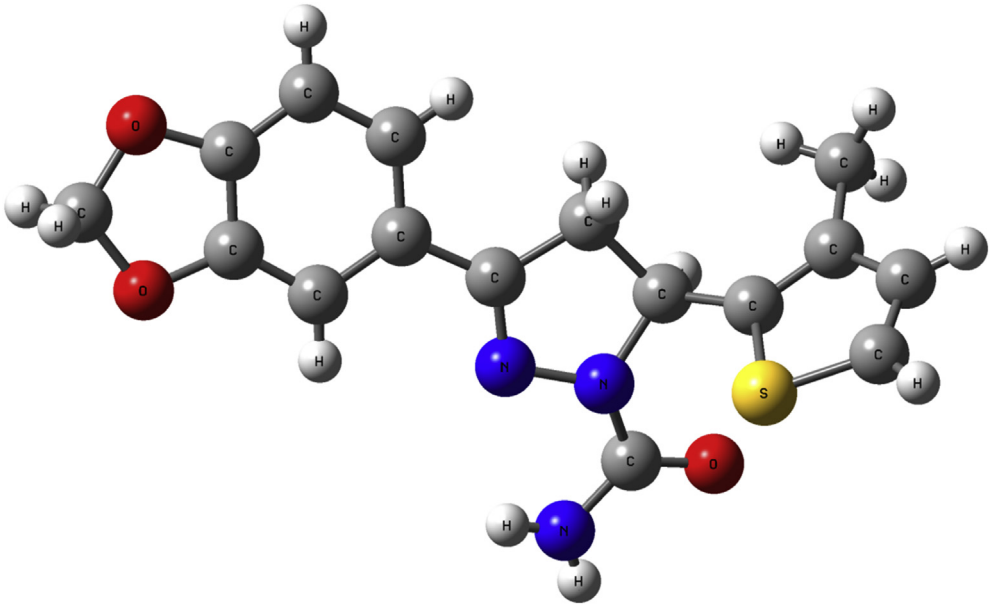

Fig. 11. Optimized structure of the title compound.

31G* and B3LYP/6-31G* methods are shown in Fig. 12. DFT geometry optimizations of the title compound was also performed with different functional (Table S5) and have observed no major changes in the values of structural parameters.

The chemical reactivity of the active sites of the molecule can be correlated to interactions with the highest occupied molecular orbital (HOMO) and lowest unoccupied molecular orbital (LUMO) of the surrounding molecules. The reactive site with higher E_{HOMO} value is ready to donate electrons to an acceptor region of lower E_{LUMO} value. Further, smaller band gap energy (ΔEgap = EHOMO - ELUMO) represents the highly reactive sites and larger band gap energy represents the poor reactive sites of the molecule. The dipole moment of the molecule is a very important factor for the correlation of the electronic properties of the molecule. If the molecule has large dipole moment, then the intermolecular interactions of the molecule are very strong. The total energy, E_{HOMO}, E_{LUMO}, the band gap (ΔE_{gap}), the ionization potential ($I = -E_{HOMO}$), the electron affinity ($A = -E_{LUMO}$), the absolute electronegativity (χ), the global hardness (η), global softness (σ), the global electrophilicity (ω), the chemical potential ($\mu = -\chi$) and the dipole moment (D) were calculated at the B3LYP/6-31 + G(d,p) level of theory [43,44] and are summarized in Table 4. The calculated HOMO and LUMO band gap energies are as shown in Fig. 13.Where $\chi = (I + A)/2$, $\eta = (I\text{-}A)/2$, $\sigma = 1/\eta$ and $\omega = \mu^2/2\eta$.

3.4.1. The Mulliken atomic charges and molecular electrostatic potential

Atomic charges were calculated using ab-initio molecular orbital calculation at B3LYP/6-31 + G(d, p) level of theory. The Mulliken atomic charges of each atom of the compound have been computed and presented (Table S6 and Fig. 14).

As seen in Fig. 14, it is evident that all the hydrogen atoms are positively charged. The hydrogen atoms attached to the N14 atom (NH_2 group) have high positive atomic charge compared with the other hydrogen atoms. The N14 atom have bigger negative (−0.76 e) charge that can be elucidated by their participation in the formation of N–H···N hydrogen bond interaction. All the oxygen atoms (O13, O19, O21) and carbon atoms (C5, C2, C8, C6) have shown high negative charges and they are readily interacts with the positively charged acceptors. C5 carbon atom have shown the highest electronegativity (−0.68 e), due to the electro-positiveness of the three surrounded hydrogen atoms. Therefore C5 is ready for electrophilic attack and the other carbons have positive charges, which would be responsible for nucleophilic attack sites [45].

The charge distribution of molecule is represented using three dimensional molecular electrostatic potential (MEP) map (Fig. 15) in between the colour scale −5.888 > a.u. (deep red) to 5.888 a.u. (deep blue). The variably charged regions of a molecule can be identified easily through colour scale, which allow us to understand how the molecules interact with one another and also the nature of their chemical bond. The positive (blue) regions of MEP represent the electrophilic reactivity and the negative (green) regions related to nucleophilic reactivity of the molecule. The red regions in the molecule were found to be regions are ready for electrophilic attack. In the figure, the negative regions are concentrated on the top of the oxygen atom and the blue regions are spread at the top of the hydrogen atoms of the NH_2 group. The remaining regions with green, yellow and smaller potential are the smaller electronegative regions.

3.4.2. Polarizability and first order hyperpolarizability calculations

The behaviour of light in nonlinear media, in which the dielectric polarization reacts nonlinearly to the electric field of the light, is called nonlinear optics (NLO). A material which possesses good NLO property has got many applications in the field of optoelectronics. DFT methods have been widely used as efficient tools for the investigation of NLO properties of organic materials [46–50]. To gathering the information about the relation between the molecular structures and NLO properties of the title compound, the polarizabilities and first order hyperpolarizabilities of the title compound were calculated using the DFT/B3LYP method and the 6-31 + G(d,p) basis set.

Further, the total molecular dipole moment (μ), linear polarizability (α) and first-order hyperpolarizability (β) were calculated [51,52] and are given in Table 5.

$$\mu_{tot} = \left(\mu_x^2 + \mu_x^2 + \mu_x^2\right)^{1/2}$$

Table 3
Theoretically calculated bond lengths (Å) and bond angles (°) of the title compound using different level of theories with different solvent environment.

Bond Lengths (Å)		XRD (EXP)	HF/3-21G	HF/6-31G*	DFT/6-31G*	DFT/6-311G*				
						GAS	DMSO	ETOH	MEOH	Acetone
S1	C6	1.7100	1.8131	1.7434	1.7535	1.751	1.7539	1.7539	1.7539	1.7099
S1	C2	1.7090	1.7923	1.7228	1.7317	1.7299	1.7365	1.7364	1.7365	1.7094
N11	N10	1.4010	1.4104	1.3728	1.3757	1.3707	1.3863	1.386	1.3861	1.4006
N11	C7	1.4810	1.4752	1.465	1.4875	1.4855	1.4847	1.4846	1.4847	1.4807
N11	C12	1.3800	1.3672	1.3689	1.3912	1.3883	1.3915	1.3919	1.3917	1.3799
O19	C18	1.3740	1.3843	1.3525	1.3704	1.3689	1.368	1.368	1.368	1.3738
O19	C20	1.4120	1.4547	1.4104	1.4348	1.4349	1.4394	1.4392	1.4392	1.4124
O21	C22	1.3700	1.3888	1.3569	1.3744	1.373	1.3726	1.3727	1.3726	1.3698
O21	C20	1.4330	1.4518	1.4074	1.4315	1.4314	1.4362	1.4362	1.4362	1.4334
O13	C12	1.2280	1.2259	1.2049	1.2271	1.2213	1.2319	1.2315	1.2317	1.2283
N10	C9	1.2900	1.2664	1.2601	1.2931	1.2898	1.2923	1.2923	1.2922	1.2903
C6	C4	1.3590	1.3391	1.3505	1.3764	1.3739	1.375	1.3749	1.375	1.3585
C6	C7	1.4980	1.4973	1.5073	1.5044	1.5046	1.5036	1.5036	1.5035	1.4983
C4	C3	1.4200	1.4525	1.4428	1.4334	1.4313	1.4376	1.4377	1.4376	1.4199
C4	C5	1.5160	1.5137	1.5093	1.5081	1.5071	1.5071	1.507	1.5071	1.5158
C7	C8	1.5360	1.555	1.5465	1.5554	1.5527	1.5557	1.5558	1.5558	1.5359
C3	C2	1.3260	1.3328	1.3415	1.3646	1.3621	1.3635	1.3635	1.3634	1.3259
N14	C12	1.3400	1.3482	1.3526	1.3684	1.3666	1.3664	1.3664	1.3663	1.3399
C8	C9	1.5000	1.5252	1.5133	1.5185	1.5194	1.5163	1.5162	1.5162	1.4997
C9	C15	1.4640	1.4668	1.4757	1.4631	1.4618	1.4639	1.4639	1.464	1.464
C15	C16	1.3970	1.3836	1.3831	1.4029	1.4006	1.4032	1.4031	1.4032	1.3972
C15	C23	1.4090	1.4056	1.4112	1.42	1.4179	1.4209	1.421	1.421	1.4093
C22	C23	1.3700	1.3563	1.3586	1.3733	1.3703	1.3737	1.3738	1.3738	1.37
C22	C18	1.3830	1.3819	1.3863	1.397	1.3956	1.3982	1.3981	1.3982	1.3827
C16	C17	1.3940	1.3971	1.4016	1.4053	1.4035	1.4056	1.4056	1.4056	1.3941
C18	C17	1.3530	1.3609	1.3626	1.3794	1.3762	1.3802	1.3803	1.3802	1.3532
Correlation Coefficient (CC)			0.9895	0.9922	0.9923	0.9922	0.9931	0.9931	0.9932	1.000

Bond Angles (°)			XRD (EXP)	HF/3-21G	HF/6-31G*	DFT/6-31G*	DFT/6-311G*				
							GAS	DMSO	ETOH	MEOH	Acetone
C6	S1	C2	91.15	89.21	91.4	91.56	91.52	91.48	91.48	91.48	91.16
N10	N11	C7	112.35	112.54	113.26	113.63	113.53	113.04	113.04	113.04	112.34
N10	N11	C12	119.86	122.41	121.23	121.09	122.41	119.84	119.85	119.84	119.86
C7	N11	C12	121.34	125.03	122.73	122.62	123.69	121.83	121.79	121.81	121.35
C18	O19	C20	106	107.35	106.75	105.97	105.62	106.18	106.17	106.18	105.95
C22	O21	C20	105.36	107.37	106.78	106.07	105.72	106.22	106.2	106.21	105.36
N11	N10	C9	108.17	108.79	109.81	109.47	109.5	109.33	109.34	109.33	108.17
S1	C6	C4	112.09	111.52	111.56	111.3	111.3	111.44	111.44	111.44	112.08
S1	C6	C7	122.16	120.64	121.14	121.08	121.11	120.02	120.02	120.02	122.16
C4	C6	C7	125.7	127.81	127.3	127.61	127.57	128.45	128.45	128.46	125.72
C6	C4	C3	111.1	113.08	111.88	111.92	111.98	111.91	111.91	111.91	111.05
C6	C4	C5	124.5	124.59	125.63	124.78	124.74	125.84	125.84	125.83	124.46
C3	C4	C5	124.5	122.31	122.49	123.29	123.27	122.25	122.25	122.25	124.46
N11	C7	C6	112.61	111.66	112.9	113.12	112.83	113.12	113.13	113.13	112.61
N11	C7	C8	101.57	100.55	101.05	100.83	100.43	101.11	101.11	101.11	101.57
C6	C7	C8	114.5	113.66	114.86	115.47	115.34	114.85	114.85	114.85	114.52
C4	C3	C2	113.7	114.58	113.49	113.79	113.74	113.75	113.74	113.74	113.73
C7	C8	C9	103	102.23	102.37	103.09	102.84	102.89	102.89	102.89	102.96
N10	C9	C8	114	113.54	113.25	112.93	112.63	113.13	113.12	113.13	114
N10	C9	C15	122.36	122.57	122.18	122.24	122.37	122.06	122.07	122.06	122.37
C8	C9	C15	123.6	123.85	124.56	124.83	124.97	124.8	124.8	124.8	123.6
C9	C15	C16	118.8	120.84	120.25	120.19	120.29	120.07	120.08	120.07	118.82
C9	C15	C23	121.3	119.08	119.65	119.94	119.97	119.97	119.96	119.96	121.27
C16	C15	C23	119.9	120.08	120.1	119.87	119.75	119.96	119.96	119.96	119.91
S1	C2	C3	112	111.6	111.67	111.42	111.47	111.43	111.43	111.43	111.96
O21	C22	C23	127.9	128.3	128.72	128.17	128.28	128.18	128.16	128.17	127.91
O21	C22	C18	110	109.62	108.9	109.48	109.38	109.54	109.54	109.54	110
C23	C22	C18	122.1	122.08	122.38	122.34	122.32	122.28	122.29	122.28	122.09
N11	C12	O13	119.6	120.98	120.97	121.26	121.13	120.78	120.78	120.78	119.55
N11	C12	N14	116.9	114.63	115.6	114.52	114.49	114.91	114.88	114.89	116.94
O13	C12	N14	123.5	124.38	123.43	124.19	124.37	124.22	124.25	124.24	123.48
C15	C16	C17	121.8	121.34	121.88	122.01	122	121.93	121.94	121.94	121.85
C15	C23	C22	116.9	117.58	117.12	117.27	117.41	117.26	117.25	117.25	116.88
O19	C18	C22	109.7	109.85	109.17	109.81	109.72	109.82	109.82	109.82	109.67
O19	C18	C17	127.9	128.57	129.06	128.55	128.73	128.5	128.5	128.51	127.91
C22	C18	C17	122.4	121.57	121.77	121.64	121.54	121.67	121.67	121.67	122.41
O19	C20	O21	108.79	105.81	107.32	108.07	107.61	107.65	107.66	107.66	108.78
C16	C17	C18	116.9	117.35	116.74	116.87	116.98	116.9	116.89	116.9	116.87
Correlation Coefficient (CC)				0.9859	0.9929	0.9934	0.9917	0.9924	0.9923	0.9924	1.0000

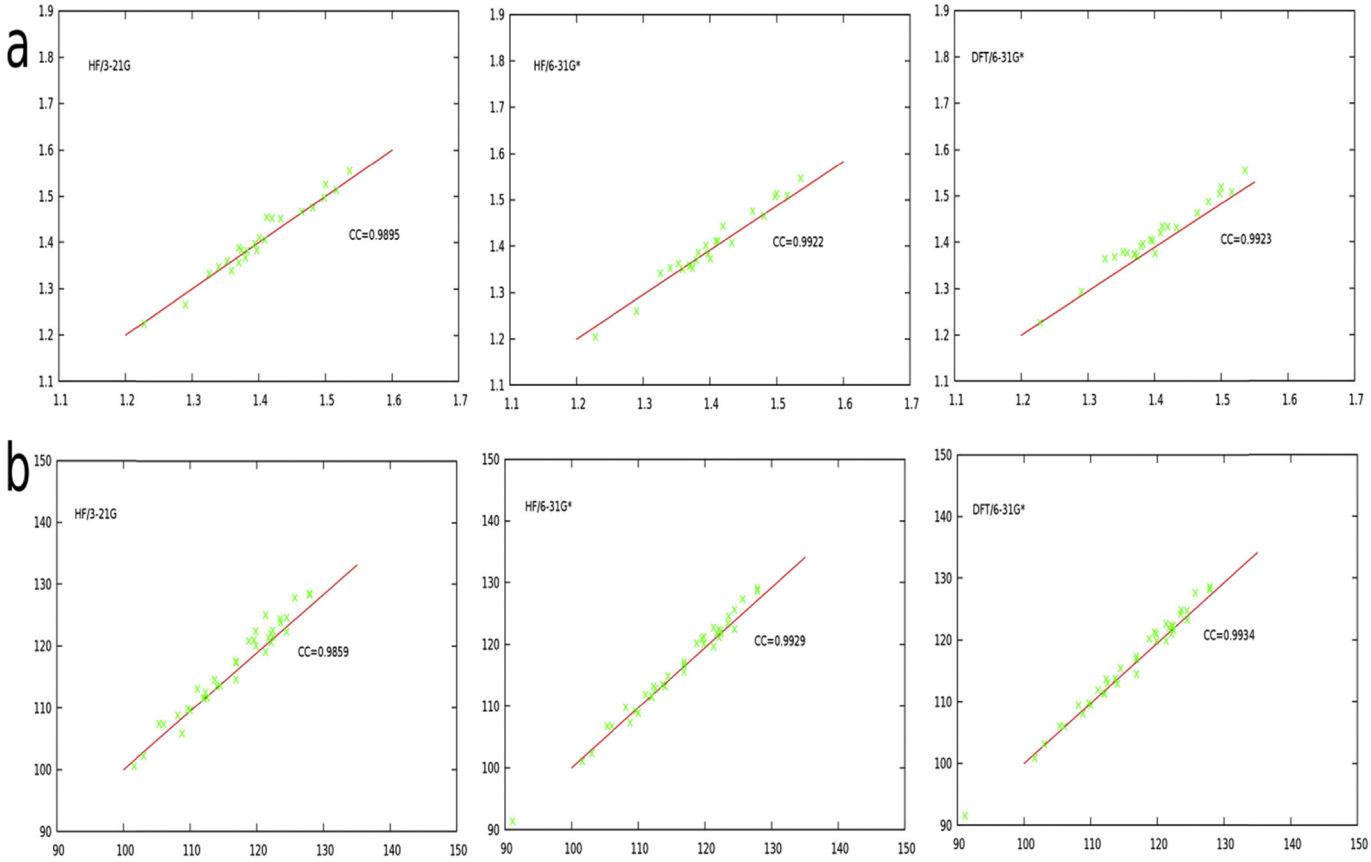

Fig. 12. Graphical correlation between experimentally determined (a) bond lengths and (b) bond angles versus the calculated values determined by HF/3-21G, HF/6-31G* and B3LYP/6-31G* methods for the title compound.

Table 4
Calculated electronic properties and quantum parameters of the title compound.

Parameters	Gas [DFT-B3LYP/6−31 G(d,p)]	Gas [DFT-B3LYP/6−311 G(d,p)]	Ethanol	Methanol	DMSO	Chloroform	Acetone
E_{HOMO}	−0.19843	−0.2059	−0.2029	−0.2029	−0.2030	−0.2007	−0.2032
E_{LUMO}	−0.04365	−0.0524	−0.0463	−0.0464	−0.0465	−0.0455	−0.0433
ΔE_{gap} (eV)	4.2116	4.1765	4.2586	4.2589	4.2589	4.2219	4.3509
Ionization potential (I)	0.19843	0.2059	0.2029	0.2029	0.2030	0.2007	0.2032
Electron affinity (A)	0.04365	0.0524	0.0463	0.0464	0.0465	0.0455	0.0433
Electronegativity (χ)	0.1210	0.1292	0.1246	0.1247	0.1248	0.1232	0.1233
Chemical hardness (η)	0.0774	0.0767	0.0783	0.0783	0.0783	0.0776	0.0800
global softness (σ)	12.9216	13.0302	12.7787	12.7779	12.7779	12.8899	12.5078
electrophilicity (ω)	0.0946	0.1088	0.0991	0.0993	0.0995	0.0978	0.0950
chemical potential(μ)	−0.1210	−0.1292	−0.1246	−0.1247	−0.1248	−0.1232	−0.1233
Dipole moment (D-Debye)	3.5161	3.4575	5.8134	5.8579	5.9032	4.6210	6.1113

The highest value of the dipole moment is observed for component μ_x (3.9998 Debye) and the lowest value of the dipole moment of the molecule is observed for the component μ_y (−1.6134 Debye). The calculated value of the total dipole moment (μ) is found to be 4.3150 Debye. The calculated average polarizability and anisotropy of the polarizability is 30.51×10^{-24} esu and 23.99×10^{-24} esu respectively. The B3LYP/6-31 + G(d,p) calculated first hyperpolarizability value (β) is 335.68×10^{-33} esu. The values of dipole moment, polarizability and hyper polarizability revealed that the title compound could be a good NLO material with potential application in the field of opto-electronics.

3.5. Thermal investigation

Thermogravimetric analysis was carried out to evaluate the thermal stability of the title compound, in nitrogen gas atmosphere. The temperature was recorded from 35 °C to 560 °C with heating rate of 10 °C min^{-1} as seen in Fig. 16. There is no weight loss around 100 °C, which evidences the absence of entrapped water in the crystal lattice or any adsorbed water on the crystal surface. The title compound displayed a good thermal stability up to 190 °C. From the TGA curve, it can be seen that the mass loss of 80% occurs in the range of 190 °C–255 °C. Initially the compound starts to decompose at 190 °C and the weight is gradually decreased up to 255 °C (residue is 20%). With the continuation of heating above

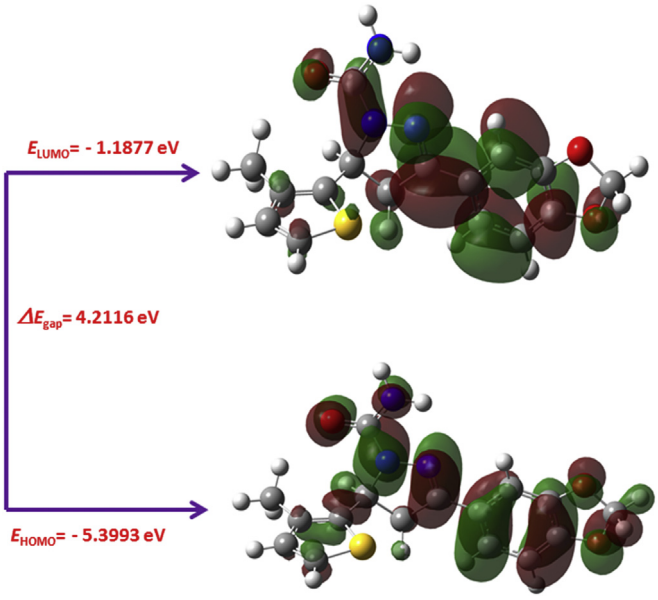

Fig. 13. HOMO and LUMO energy plot of the title compound.

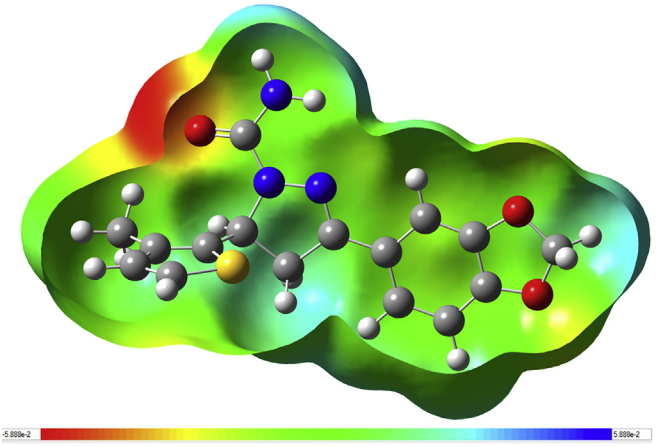

Fig. 15. MEP of the title compound.

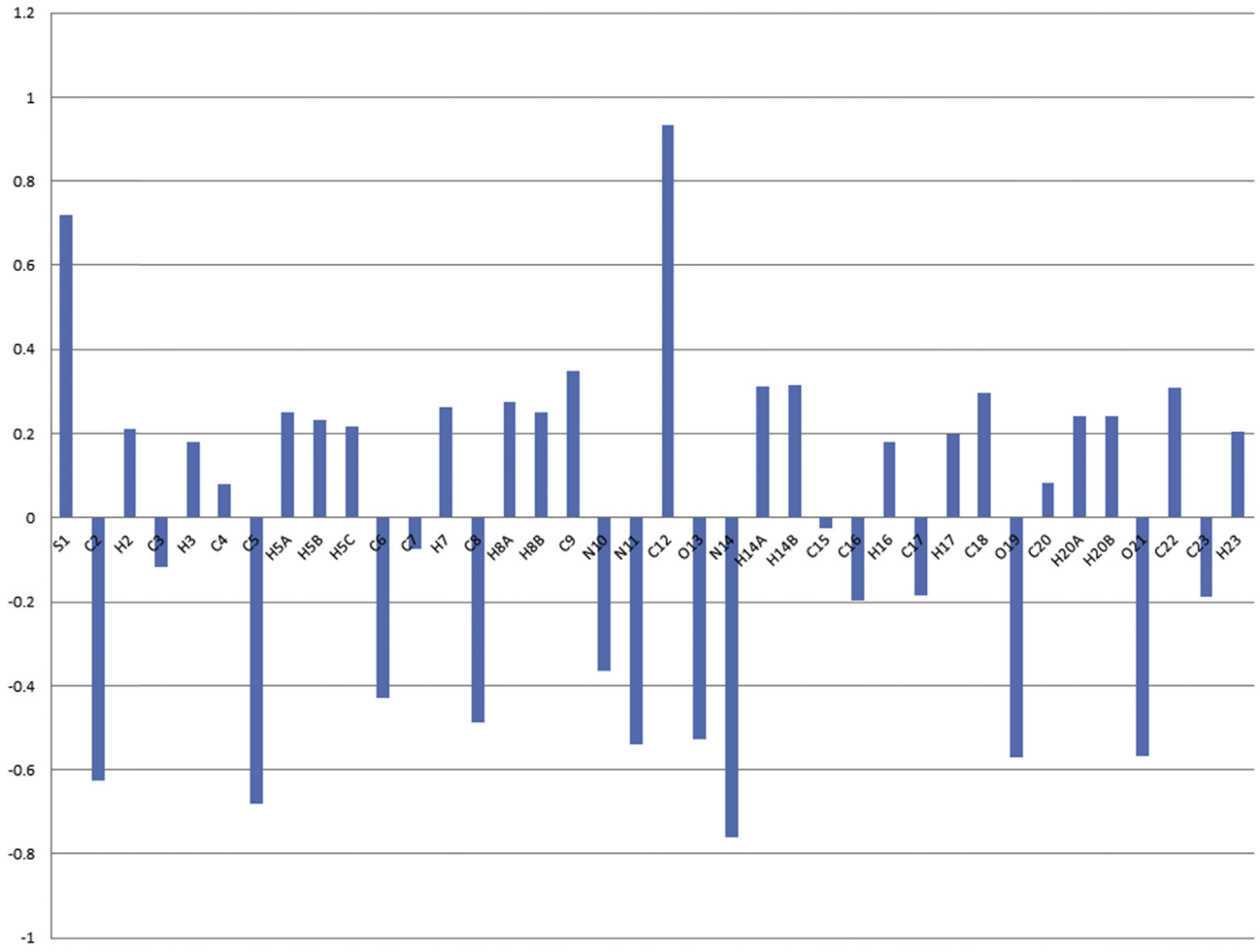

Fig. 14. Mulliken atomic charges of the title compound.

Table 5
The electronic dipole moment (μ) (Debye), polarizability (α) and first hyperpolarizability (β) of the title compound.

Parameter	a.u.	Parameter	a.u.
α_{xx}	305.772	β_{xxx}	153.142
α_{xy}	−5.609	β_{xxy}	−186.054
α_{yy}	183.710	β_{xyy}	−90.879
α_{xz}	8.589	β_{yyy}	−5.8509
α_{yz}	19.382	β_{xxz}	2.4284
α_{zz}	128.170	β_{xyz}	28.2762
α_{total}	30.51×10^{-24} esu	β_{yyz}	−41.6633
$\Delta\alpha$	23.99×10^{-24} esu	β_{xzz}	−24.8110
μ_x	3.998	β_{yzz}	−25.2915
μ_y	−1.613	β_{zzz}	29.2800
μ_z	0.1333	β_{total}	335.68×10^{-33} esu
μ_{total}	4.315		

450 °C, 15% of the residue is left out due to the charring of the carbon. The compound decomposed completely after 560 °C.

4. Conclusion

The novel pyrazole derivative (3-(benzo[d] [1,3]dioxol-5-yl)-5-(3-methylthiophen-2-yl)-4,5-dihydro-1H-pyrazole-1-carboxamide) was synthesized and characterized by means of various spectroscopic tools like: FT-IR, NMR (^{1}H and ^{13}C), MS, UV–visible spectrum and finally the three dimensional structure of the title compound was confirmed by single crystal X-ray diffraction studies. The pyrazole ring adopts an *E*-form and an envelope conformation on C7 atom. Crystal structure revealed the three dimensional supramolecular self-assembly, in which C–H···O and N–H···O chains build up two dimensional arrays, which are extended to 3D network through C–H···*Cg* and C–O···*Cg* interactions. Intra molecular N–H···N and π···π stacking interactions, contributes to the structural stability. The three dimensional d_{norm} and 2D FP plots from HSA were studied

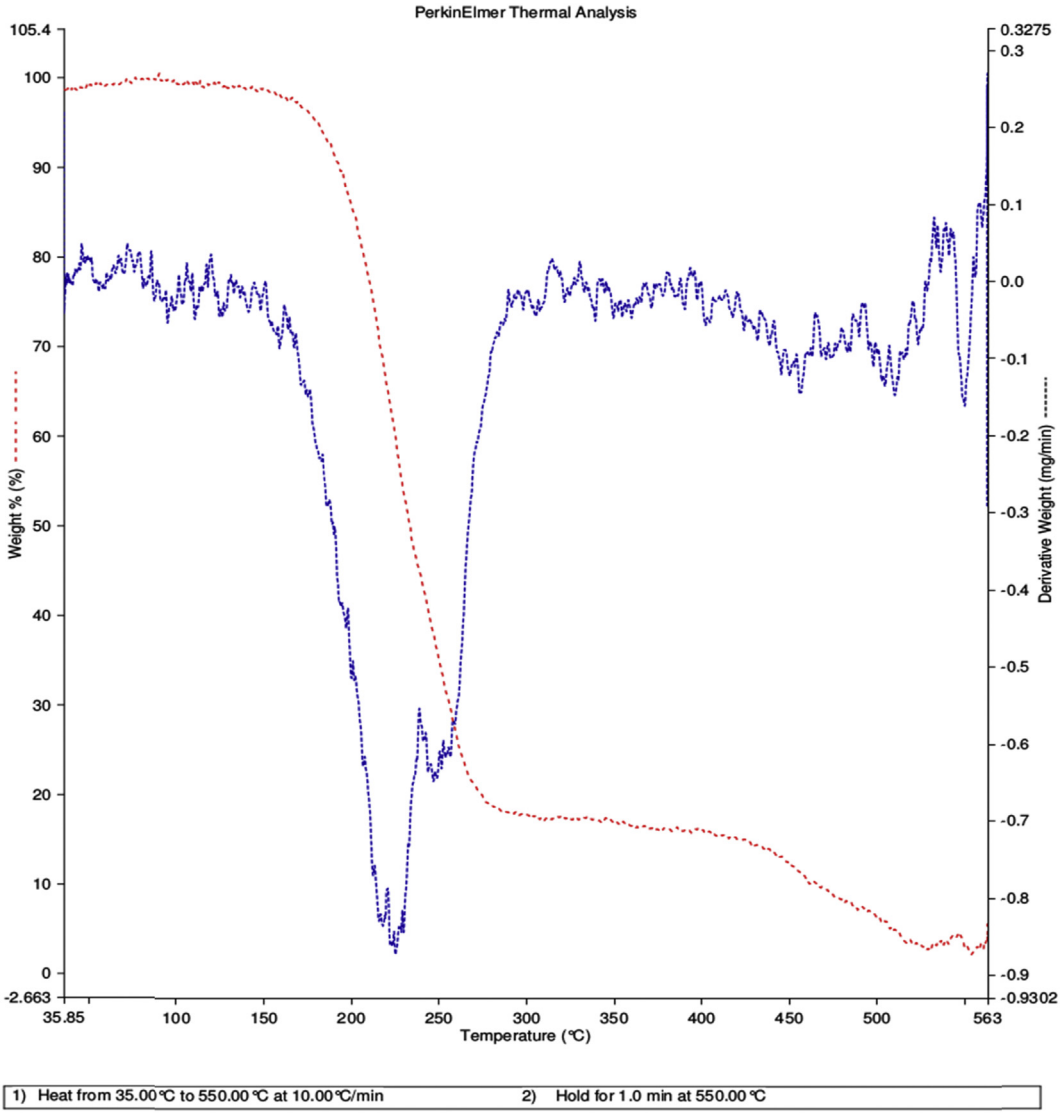

Fig. 16. TG-DTG curve of the title compound.

extensively to understand the intermolecular interactions. The HSA disclosed that H···H interactions has maximum contribution to the total Hirshfeld surface. Optical and thermal properties of the title compound were studied by UV–Vis spectroscopy and TGA. The compound exhibits a good thermal stability up to 190 °C and decomposed completely at 560 °C.

Further, the molecule was geometrically optimized using B3LYP/6-31G(d,p) level of theory. The calculations were repeated at different solvent environment to study the solvent effect on the structural parameters. The correlation coefficient between the bond lengths and bond angles of experimental and theoretical values showed that the structure obtained by the single crystal XRD is well agreed with the optimized structure. However, the acetone environment gives highest correlation coefficient amongst the other solvent. The electronic transitions between the molecular orbitals were studied using TD-DFT at the same level of theory. The band gap energy calculated from UV–Vis absorption spectrum (4.2034 eV) agree with the theoretically calculated value (4.2116 eV). The Mulliken atomic charges and MEP were analysed for the nucleophilic and electrophilic regions of the molecular surface. The Hirshfeld surface and MEP analysis consisted with presence of a strong N–H···N hydrogen bonding formation. The non-linear optical properties of the title compound were also discussed based on the linear polarizability and first order hyperpolarizability values obtained from the DFT calculation, which concludes that the title compound might be a good NLO material.

Acknowledgments

The authors are grateful to the National Single Crystal Diffractometer Facility, Department of Studies in Physics, University of Mysore, Manasagangotri, Mysuru for providing X-ray intensity data. The authors acknowledge the financial support of IOE, UPE and DST-PURSE projects.

Appendix A. Supplementary data

Supplementary data related to this article can be found at https://doi.org/10.1016/j.molstruc.2018.02.068

References

[1] K. Vinod, K. Kamalneet, K.G. Girish, K.S. Anil, Eur. J. Med. Chem. 69 (2013) 735–753.
[2] C. Franco, M. Elias, S. Daniela, B. Adriana, C. Paola, G. Arianna, B. Olivia, T. Paola, A. Stefano, O. Francesco, C. Roberto, L.T. Francesco, C.C. Maria, D. Simona, J. Med. Chem. 48 (2005) 7113–7122.
[3] S.K. Rangappa, C. Karam, T. Ramakrishnappa, B.M. Nagaraja, Arch. Pharm. Chem. Life 348 (2015) 299–314.
[4] N. Renuka, G. Pavithra, K. Ajay Kumar, Der. Pharma Chem. 6 (1) (2014) 482–485.
[5] M.G. Prabhudeva, M. Prabhuswamy, A. Dileep Kumr, N.K. Lokanath, S. Naveen, K. Ajay Kumar, Chem. Data Coll. 9–10 (2017) 80–88.
[6] N. Kaur, D. Kishore, J. Chem. Sci. 125 (3) (2013) 555–560.
[7] M. Prabhuswamy, Kumara Karthik, G. Pavithra, K. Ajay kumar, N.K. Lokanath, Chem. Data Coll. 3–4 (2016) 26–35.
[8] K.R. Raghavendra, N. Renuka, H.K. Vivek, S. Bharath, K. Ajay kumar, S. Shashikanth, Bioorg. Med. Chem. Lett. 26 (2016) 3621–3625.
[9] R.J. Lewis Sr. (Ed.), Hawley's Condensed Chemical Dictionary, twelfth ed., Van NostrandRheinhold Co, New York (, 1993, p. 860.
[10] D. Hartley, H. Kidd (Eds.), The Agrochemicals Handbook, Royal Society of Chemistry/Unwin Brothers Ltd, Old Woking Surrey, United Kingdom, 1983.
[11] W. Gerhartz, Ullmann's Encyclopedia of Industrial Chemistry, fifth ed., VCH Publishers, Deerfield Beach FL, 1985.
[12] C. Lee, W. Yang, R.G. Parr, Phys. Rev. B 37 (1988) 785–790.
[13] A.D. Becke, J. Chem. Phys. 98 (1993) 5648–5652.
[14] Chemcraft 1.6 software, http://www.chemcraftprog.com.
[15] R. Ennington, T. Keith, J. Millam, Shawnee Mission KS, GaussView, Semichem Inc, 2009, Version 5.0. .
[16] S.K. Wolff, D.J. Grimwood, J.J. McKinnon, D. Jayatilaka, M.A. Spackamn, Crystal Explorer 3.1, University of Western Australia, Perth, Australia, 2007.
[17] Rigaku, Crystal Clear, Rigaku Corporation, Tokyo, Japan, 2011.
[18] G.M. Sheldrick, Acta Cryst. C71 (2015) 3–8.
[19] A.L. Spek, Acta Cryst. A46 (1990) c34–c34.
[20] C.F. Macrae, I.J. Bruno, J.A. Chisholm, P.R. Edgington, P. McCabe, E. Pidcock, L.M. Rodriguez, R. Taylor, J. van de Streek, P.A. Wood, J. Appl. Cryst. 41 (2008) 466–470.
[21] S. Suresh, Opt. Int. J. Light Electron Opt. 125 (12) (2014) 2826.
[22] X.F. Shi, C.Y. Liu, Bo Liu, C.C. Yuan, Acta Cryst. E63 (2007) o1295–o1296..
[23] H.A. Skinner, Rev. Port. Quim. 29 (39) (1987) 39–46.
[24] D.T. Cremer, J.A. Pople, J. Am. Chem. Soc. 97 (6) (1975) 1354–1358.
[25] S.T. Rao, E.T. Westhof, M. Sundaralingam, Acta Cryst. A37 (1981) 421–425.
[26] P.I. Nagy, Int. J. Mol. Sci. 15 (11) (2014) 19562–19633.
[27] J. Bernstein, R.E. Davis, L. Shimoni, N.-L. Chang, Int. Ed. 34 (1995) 1555–1573.
[28] M.A. Spackman, D. Jayatilaka, CrystEngComm 11 (2009) 19–32.
[29] Kumara Karthik, S. Naveen, L.D. Mahadevaswamy, A.K. Kariyappa, N.K. Lokanath, Chem. Data Coll 9 (2017) 251–262.
[30] Kumara Karthik, M. Jyothi, S. Naveen, Zabiulla, S.A. Khanum, N.K. Lokanath, Chem. Data Coll 9–10 (2017) 152–163.
[31] D. Jayatilaka, D.J. Grimwood, A. Lee, A. Lemay, A.J. Russell, The University of Western Australia, Nedlands, 2005 .
[32] S.K. Seth, CrystEngComm 15 (2013) 1772–1781.
[33] S.K. Seth, J. Mol. Struct. 1064 (2014) 70–75.
[34] Y.H. Luo, G.G. Wu, S.L. Mao, B.W. Sun, Inorg. Chim. Acta. 397 (2013) 1–9.
[35] P.M. Dean, J.M. Pringle, C.M. Forsyth, J.L. Scott, D.R. MacFarlane, New J. Chem. 32 (2008) 2121–2126.
[36] K. Fukui, Science 218:4574 (1982) 747–754.
[37] A. Lesar, I. Miosev, Chem. Phys. 483 (2009) 198–203.
[38] G.A. Petersson, T.G. Tensfeldt, J.A. Montgomery, J. Chem. Phys. 94 (1991) 6091–6101.
[39] W.J. Hehre, R.F. Stewart, J.A. Pople, J. Chem. Phys. 51 (1969) 2657–2664.
[40] P. Pulay, G. Fogarasi, F. Pang, J.E. Boggs, J. Am. Chem. Soc. 101 (1979) 2550–2560.
[41] R.G. Parr, L.V. Szentpaly, S. Liu, J. Am. Chem. Soc. 121 (1999) 1922–1924.
[42] R.G. Parr, R.A. Donnelly, M. Levy, W.E. Palke, J. Chem. Phys. 68 (1978) 3801–3807.
[43] I. Warad, F.F. Awwadi, M. Daqqa, A. Al Ali, T.S. Ababneh, T.M. AlShboul, Y.N. Mabkhot, J. Photochem. Photobiol. B Biol. 171 (2017) 9–19.
[44] S. Xavier, S. Periandy, S. Ramalingam, Spectrochim. Acta Mol. Biomol. Spectrosc. 137 (2015) 306–320.
[45] J.H. Zhou, L.W. Zheng, M.C. Yan, M.J. Shi, J. Liu, G.Q. Shangguan, J. Chem. (2017), 6537402, 9 pages, https://doi.org/10.1155/2017/6537402.
[46] Y.X. Sun, Q.L. Hao, Z.X. Yu, W.X. Wei, L.D. Lu, X. Wang, Mol. Phys. 107 (2009) 223–235.
[47] A.B. Ahmed, H. Feki, Y. Abid, H. Boughzala, C. Minot, A. Mlayah, J. Mol. Struct. 920 (2009) 1–7.
[48] J.P. Abraham, D. Sajan, V. Shettigar, S.M. Dharmaprakash, I. Nemec, I.H. Joe, V.S. Jayakumar, J. Mol. Struct. 917 (2009) 27–36.
[49] S.G. Sagdinc, A. Esme, Spectrochim. Acta Part A 75 (2010) 1370–1376.
[50] A.B. Ahmed, H. Feki, Y. Abid, H. Boughzala, C. Minot, Spectrochim. Acta Part A 75 (2010) 293–298.
[51] K.S. Thanthiriwatte, K.M. Nalin de Silva, J. Mol. Struct. 617 (2002) 169–175.
[52] Y. Jiang, L. Zi Zhong, L. Hong Xia, C. Wen Ying, N. WANG, L. Dong Sheng, G. Xiang Wei, Chin. Sci. Bull. 57 (34) (2012) 4448–4452.